THE JOURNAL OF PHYSICAL CHEMISTRY LETTERS
A JOURNAL OF THE AMERICAN CHEMICAL SOCIETY

pubs.acs.org/JPCL

Letter

Rotational Spectrum of the Phenoxy Radical

P. Bryan Changala* and Michael C. McCarthy*

Cite This: J. Phys. Chem. Lett. 2024, 15, 5063−5069

Read Online

ACCESS | Metrics & More | Article Recommendations | Supporting Information

ABSTRACT: We report the hyperfine-resolved rotational spectrum of the gas-phase phenoxy radical in the 8−25 GHz frequency range using cavity Fourier transform microwave spectroscopy. A complete assignment of its complex but well-resolved fine and hyperfine splittings yielded a precisely determined set of rotational constants, spin-rotation parameters, and nuclear hyperfine coupling constants. These results are interpreted with support from high-level quantum chemical calculations to gain detailed insight into the distribution of the unpaired π electron in this prototypical resonance-stabilized radical. The accurate laboratory rest frequencies enable studies of the chemistry of phenoxy in both the laboratory and space. The prospects of extending the present experimental and theoretical techniques to investigate the rotational spectra of isotopic variants and structural isomers of phenoxy and other important gas-phase radical intermediates that are yet undetected at radio wavelengths are discussed.

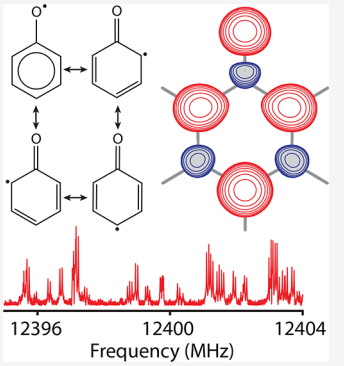

The phenoxy radical (C_6H_5O) is an important intermediate in the formation and decomposition of oxidized aromatic hydrocarbons in gas-phase combustion, pyrolysis, and atmospheric environments.[1−4] At high-temperature conditions, phenyl radicals (C_6H_5) react efficiently with O_2 to produce phenoxy,[4−6] a process that removes carbon mass from further reactions that otherwise lead to the formation and growth of polycyclic aromatic hydrocarbons (PAHs).[7] Aryl ethers, such as anisole, and other model compounds for lignin, a major component of biomass, thermally decompose to phenoxy, which itself fragments into smaller radicals, including cyclopentadienyl (C_5H_5) and propargyl (CH_2CCH).[8−10] Because phenoxy can be formed and destroyed by barrierless, exothermic reactions, it may also play an important role in the first stages of PAH chemistry in low-temperature, interstellar environments, including cold molecular clouds.[11] The delocalization of the unpaired electron throughout the π system of the O atom and adjoining six-membered aromatic ring has a profound influence on the reactivity of phenoxy. Like other resonance-stabilized radicals, phenoxy is relatively long-lived, immune to O_2 addition and attack,[2,3] and can build up to high concentrations in reactive environments. Probing these aspects of its chemical structure and reaction kinetics has been a primary motivation for spectroscopic studies of phenoxy using a variety of methods. Condensed-phase electron spin resonance (ESR) studies[12−17] have confirmed the delocalized nature of the unpaired electron, while anion and neutral photoelectron spectroscopy,[18−23] ultraviolet (UV)/visible absorption measurements,[2,3,24−27] and matrix-isolation infrared (IR) spectroscopy[10,28] have provided valuable insight into its thermochemistry and vibronic structure.

In light of the long-standing interest in phenoxy as a prototypical resonance-stabilized π radical, it is perhaps surprising that its microwave rotational spectrum remains unknown, despite efficient methods for synthesizing phenoxy in the gas phase and its large permanent dipole moment ($\mu \sim 3.7$ D), which favors detection by this means. One factor hindering its microwave detection at high spectral resolution is the complex splittings expected in its rotational spectrum as a result of the spin-rotation fine structure, which couples the electronic spin ($S = 1/2$) with the rotational angular momentum, and the nuclear magnetic hyperfine structure, which couples the hydrogen nuclear spins ($I_H = 1/2$) with the electronic spin, similar to that observed in phenyl.[29] Indeed, although tentative evidence of the rotational spectrum of phenoxy was recently reported in our laboratory during the analysis of the products of a $C_6H_6 + O_2$ electric discharge with broadband microwave spectroscopy,[30] no definitive assignments were attempted owing to the intricate, closely spaced line structure.

In this letter, we report new measurements of the putative phenoxy rotational transitions with cavity Fourier transform microwave (FTMW) spectroscopy in the 8−25 GHz frequency range. The high spectral resolution and detection sensitivity of cavity FTMW have enabled the unambiguous assignment of the observed spectrum, including the extensive and well-resolved fine and hyperfine structure, to phenoxy. Our results are supported by theoretical predictions of the rotation, spin-rotation, and nuclear hyperfine parameters derived from high-level quantum chemical calculations of the equilibrium

Received: April 1, 2024
Revised: April 28, 2024
Accepted: May 1, 2024
Published: May 3, 2024

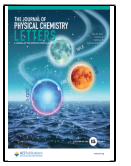

https://doi.org/10.1021/acs.jpclett.4c00962
J. Phys. Chem. Lett. 2024, 15, 5063−5069

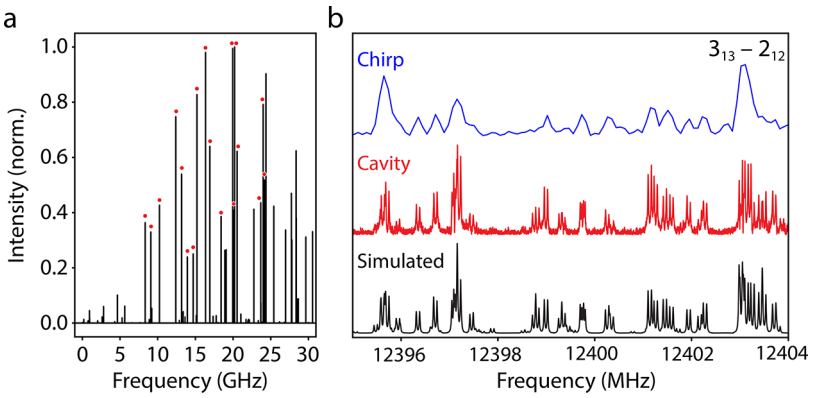

Figure 1. Microwave spectrum of phenoxy. (a) Simulated spectrum of the 0−30 GHz frequency range assuming T_{rot} = 2 K. The 18 rotational transitions measured in this study are marked with red dots. (b) Simulated (bottom, black) and measured (middle, red) fine/hyperfine structure of the $N_{K_aK_c} = 3_{13} - 2_{12}$ rotational transition centered near 12.4 GHz. The measured cavity spectrum is a concatenation of 30 individual spectra, each of which is 0.3 MHz wide and integrated for 1 min. The same frequency region from the broadband chirped-pulse FTMW spectrum of a benzene + O_2 discharge reported by McCarthy et al.[30] is included for comparison (top, blue). The cavity measurements have a double-peaked line profile arising from the Doppler effect as the gas expands along the axis of the Fabry−Pérot cavity. Each of the two Doppler sidebands has a full width at half maximum (fwhm) of ≈10 kHz, which is 15× narrower than the chirped-pulse line profile (fwhm of ≈150 kHz).

geometry, zero-point vibrational effects, and electronic wave function. In addition to providing detailed insight into the ground-state structure and π delocalization of phenoxy, the experimentally derived spectroscopic constants can be used to calculate an accurate (ca. 1 kHz) hyperfine-resolved line list in the centimeter wave band. These data enable the sensitive and selective detection of phenoxy in a variety of complex mixtures and reaction environments by microwave techniques. The derived rest frequencies are also of sufficient accuracy to search for evidence of phenoxy in radio astronomical surveys of narrow line width interstellar sources, such as dark, cold molecular clouds.[31,32] More broadly, these results demonstrate an effective strategy for the microwave detection and analysis of other important aromatic and resonance-stabilized radical intermediates.

Gas-phase phenoxy radicals were generated in an electric discharge expansion and detected with a cavity FTMW spectrometer operating from 5 to 40 GHz.[33] A dilute mixture of either benzene/O_2 or anisole ($C_6H_5OCH_3$) in neon was supersonically expanded into a large vacuum chamber containing a confocal microwave cavity. As the gas enters the chamber, it passes through two copper ring electrodes biased with a 700−1000 V potential, which produces a 20−40 mA discharge current. Rotational transitions of phenoxy were excited by a short pulse of resonant microwave radiation, and the resulting free induction decay (FID) was detected with a sensitive microwave receiver. The rest frequencies of the transitions were measured to an accuracy of 2 kHz. Further details are provided in the Experimental Methods.

A total of 18 pure rotational transitions ($N \leq 6$ and $K_a \leq 3$) were measured in the 8−25 GHz frequency range. Each transition is split into a dense cluster of fine/hyperfine components spanning a ∼10 MHz window (Figure 1). The complex splittings of each pure rotational transition were assigned with guidance from the theoretical predictions of the spin-rotation and nuclear hyperfine coupling constants (see below), the measured relative intensities, and the Zeeman splitting patterns observed with an applied magnetic field. A total of ∼300 individual hyperfine-resolved transitions were used to fit an effective Hamiltonian containing the rotational constants (A, B, and C), quartic centrifugal distortion parameters (Δ_N, Δ_{NK}, Δ_K, δ_N, and δ_K), spin-rotation coupling tensor elements (ϵ_{aa}, ϵ_{bb}, and ϵ_{cc}), and both isotropic (a_F) and diagonal anisotropic (T_{aa} and $T_{bb} - T_{cc}$) hyperfine coupling constants for each H nucleus. The two equivalent pairs of *ortho* and *meta* H atoms have identical hyperfine parameters, resulting in a total of 18 free parameters (Δ_K and δ_K were poorly determined and, therefore, were held fixed to their *ab initio* values). Tables 1 and 2 summarize the best fit experimental parameters optimized with the SPFIT program.[34] The root-mean-square (rms) fit error is 3.5 kHz. The complete experimental line list and fit information is available in the Supporting Information.

Table 1. Rotation, Centrifugal Distortion, and Spin-Rotation Constants of Phenoxy in the A-Reduced I^r Representation[a]

parameter	measured	calculated
A	5486.9020(14)	5485.11[b]
B	2793.0189(2)	2789.56[b]
C	1850.9540(1)	1849.37[b]
$\Delta_N \times 10^3$	0.157(3)	0.1509[c]
$\Delta_{NK} \times 10^3$	0.16(2)	0.1887[c]
$\Delta_K \times 10^3$	[1.0363][d]	1.0363[c]
$\delta_N \times 10^3$	0.053(2)	0.0517[c]
$\delta_K \times 10^3$	[0.3625][d]	0.3625[c]
ϵ_{aa}	−99.466(3)	−93.57[e]
ϵ_{bb}	−13.213(1)	−13.12[e]
ϵ_{cc}	−0.0859(5)	+0.85[e]

[a]All values are in MHz with 1σ uncertainties given in parentheses in units of the last digit. [b]The best estimate values derived from the frozen-core ROHF-CCSD(T)/cc-pVQZ equilibrium geometry plus a core−valence correlation correction [equal to the difference of the all-electron and frozen-core ROHF-CCSD(T)/cc-p(C)VTZ equilibrium constants] and vibrational zero-point corrections [calculated with VPT2 at the UHF-CCSD(T)/cc-pVTZ level of theory]. [c]Harmonic ROHF-CCSD(T)/cc-pVTZ values. [d]Fixed to the calculated value. [e]Spin-rotation parameters calculated at the UHF-CCSD(T)/cc-pVTZ level of theory.

The theoretical equilibrium geometry of phenoxy was optimized with coupled cluster theory, including single, double, and perturbative triple excitations [CCSD(T)][36,37] based on

https://doi.org/10.1021/acs.jpclett.4c00962
J. Phys. Chem. Lett. 2024, 15, 5063−5069

Table 2. Hydrogen Hyperfine Coupling Constants of Phenoxy[a]

parameter[b]	this work	ESR[c]	ESR[d]	calculated[e]
o-a_F	−20.390(2)	−18.5(1)	−19.23(6)	−20.516
o-T_{aa}	−5.767(2)			−6.153
o-$T_{bb} - T_{cc}$	8.593(5)			9.339
m-a_F	6.338(4)	5.2(1)	5.63(6)	7.402
m-T_{aa}	1.401(2)			1.949
m-$T_{bb} - T_{cc}$	4.847(7)			4.136
p-a_F	−28.261(3)	−28.6(1)	−27.80(6)	−28.050
p-T_{aa}	14.670(2)			15.449
p-$T_{bb} - T_{cc}$	−16.424(8)			−16.686

[a]All values are in MHz with 1σ uncertainties given in parentheses in units of the last digit. [b]o = *ortho*, m = *meta*, and p = *para*. [c]Electron spin resonance measurement in aqueous solution.[35] The sign is inferred from the gas-phase values measured in this work. [d]Electron spin resonance measurement in benzene solution.[17] The sign is inferred from the gas-phase values measured in this work. [e]Equilibrium values at the ROHF-CCSD(T)/cc-pVTZ level of theory.

both unrestricted (UHF)[38] and restricted open-shell (ROHF)[39,40] reference wave functions and the correlation-consistent polarized valence basis sets (cc-pVXZ)[41] and core−valence basis sets (cc-pCVXZ)[42] for frozen-core and all-electron calculations, respectively. Harmonic centrifugal distortion constants and anharmonic vibration−rotation constants [derived via second-order vibrational perturbation theory (VPT2)[43]] were calculated with quadratic and cubic force fields constructed by finite differences of analytic gradients. First-order electronic properties, including the electric dipole moment and hyperfine coupling constants, were calculated at the UHF and ROHF optimized equilibrium geometries via analytic first-derivative techniques, while spin-rotation constants[44] were calculated only for UHF reference wave functions for which analytic second-derivative methods are available.[45] All calculations were performed with the CFOUR program package.[46,47] The calculated rotation, centrifugal distortion, spin-rotation, and nuclear hyperfine parameters are listed alongside the respective experimental values in Tables 1 and 2 (see Table S1 of the Supporting Information for the optimized structural parameters). The excellent agreement between the measured and theoretical constants provides a high degree of confidence in the phenoxy assignment.

The observed nuclear spin statistics of the well-resolved hyperfine structure provide additional experimental evidence for the assignment. The unpaired electron in phenoxy occupies a π orbital of b_1 symmetry in the C_{2v} point group, resulting in a $^2B_1$ electronic ground state. The two *ortho* H nuclear spins ($I = 1/2$) couple to form an intermediate composite spin $I_o = 0$ or 1. Similarly, the two *meta* H nuclear spins couple to form $I_m = 0$ or 1. Fermionic statistics require that the permutation of either of the *ortho* or *meta* pairs changes the sign of the total spin-rovibronic wave function. Thus, in rotational states with K_a = even, only hyperfine states with $(I_o, I_m) = (0, 1)$ or $(1, 0)$ exist, while in rotational states with K_a = odd, only hyperfine states with $(I_o, I_m) = (0, 0)$ or $(1, 1)$ exist. The observed spectra do, in fact, exhibit these spin selection rules, consistent with the expected $^2B_1$ electronic symmetry.

The precisely determined rotation, spin-rotation, and nuclear hyperfine parameters reveal detailed insights into the structure and electronic properties of phenoxy. Although the lack of data from isotopically substituted species prevents a complete (semi)experimental equilibrium structure determination at this juncture, the good agreement (~0.1%) between the measured and best estimate theoretical rotational constants (Table 1) lends confidence to the accuracy of the corresponding theoretical equilibrium structure, which is illustrated in Figure 2.

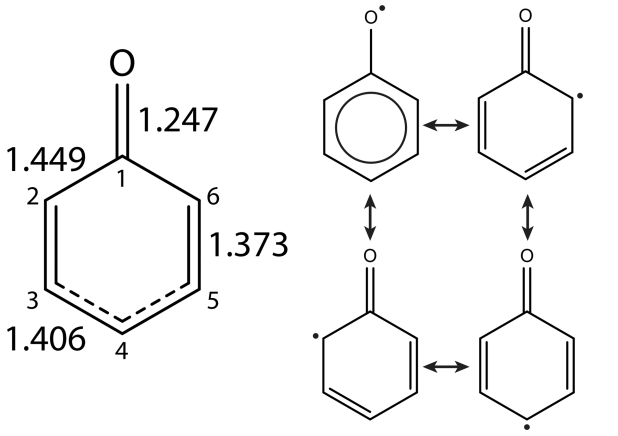

Figure 2. Structure of phenoxy. The theoretical equilibrium bond lengths of the heavy-atom skeleton {ROHF-CCSD(T)/cc-pVQZ + core-correlation correction [ROHF-CCSD(T)/cc-p(C)VTZ]} in angstroms are shown alongside the electronic resonance structures.

The calculated C− C bond lengths show significant differences from their reference semi-experimental equilibrium values in a normal benzene ring [r_{CC} = 1.3913(3) Å[48]]. As the accompanying resonance structures illustrate, the delocalization of the unpaired π electron in phenoxy results in an approximate O− C_1 double bond (1.247 Å), a C_1− C_2 single bond (1.449 Å), a C_2− C_3 double bond (1.373 Å), and an intermediate C_3− C_4 single/double bond (1.406 Å).

The H hyperfine coupling parameters provide an even more direct and quantitative probe of the delocalization of the unpaired π electron. The isotropic Fermi contact constants (a_F) derived in this work are approximately 2 orders of magnitude more precise than previous ESR measurements in condensed-phase samples[12−17] (Table 2). Although the gas- and condensed-phase values are similar, they exhibit small but measurably significant differences owing to condensed-phase environmental effects that perturb the molecular electronic structure. The primary contribution to the a_F parameter for each H nucleus arises from spin polarization of the H σ(1s) electrons by the unpaired spin population (ρ) in the neighboring C π(2p) orbital. A well-known approximate, empirical relationship[49,50] between these two quantities is

$$a_F \approx -63\ \text{MHz} \times \rho \quad (1)$$

The spin populations of the hydrogen-bonded C atoms derived from this expression are listed in Table 3. Our results also include the anisotropic H hyperfine coupling constants (T_{aa}, T_{bb}, and T_{cc}), reported here apparently for the first time. Similar approximate expressions[51] also relate the in-plane (a and b axes) anisotropy parameters to the adjacent C spin population

$$T_{aa} \approx (43.3\ \text{MHz} \times \cos^2\theta - 38.7\ \text{MHz} \times \sin^2\theta)\rho \quad (2)$$

$$T_{bb} \approx (43.3\ \text{MHz} \times \sin^2\theta - 38.7\ \text{MHz} \times \cos^2\theta)\rho \quad (3)$$

where θ is the angle between the CH bond vector and the principal a axis (which is parallel to the CO bond). The spin populations derived from T_{aa} and T_{bb}, assuming that the bond

https://doi.org/10.1021/acs.jpclett.4c00962
J. Phys. Chem. Lett. 2024, 15, 5063−5069

Table 3. Unpaired Spin Populations in Phenoxy

atom	$\rho(a_F)^a$	$\rho(T_{aa})^b$	$\rho(T_{bb})^b$	calculated[c]
O				+0.41
C_1				−0.09
$C_{2,6}$	+0.32	+0.35	+0.34	+0.30
$C_{3,5}$	−0.10	−0.08	+0.08	−0.13
C_4	+0.45	+0.34	+0.40	+0.39

[a]Spin populations derived from the H a_F parameters using eq 1. [b]Spin populations derived from the H T_{aa} and T_{bb} parameters using eqs 2 and 3. [c]Total atomic spin populations calculated at the ROHF-CCSD(T)/cc-pVTZ level of theory.

angles equal our best estimate equilibrium values [$\theta(C_2H)$ = 58.5° and $\theta(C_3H)$ = 120.1°; $\theta(C_4H)$ = 180.0° exactly by symmetry], are listed in Table 3, which also includes the theoretical Mulliken spin populations from the ground-state electronic wave function. The large positive spin populations on the O, C_2, C_4, and C_6 atoms are consistent with qualitative expectations based on the resonance forms in Figure 2. These resonance structures also illustrate why the inconsistency in sign and magnitude among the empirical and *ab initio* results is greatest for the *meta* positions (C_3 and C_5). The spin population at these atoms is itself dominated by spin polarization from the large positive spin density at the adjacent atoms (C_2, C_4, and C_6). The resulting hyperfine coupling constants at the *meta* H nuclei are therefore influenced by both first- and second-order spin-polarization contributions from the nearest neighbor and next nearest neighbor C atoms.[52] Only the former is accounted for by eqs 1−3.

The spin-rotation parameters (ϵ_{aa}, ϵ_{bb}, and ϵ_{cc}) reveal additional insight into the excited electronic manifold of phenoxy. Under the (usually good) approximation that these parameters are dominated by second-order spin−orbit interactions that mix small amounts of electronic orbital angular momentum into the ground-state wave function, the ϵ_{ii} tensor elements are directly proportional to the magnetic g-tensor anisotropy, $\epsilon_{ii} = 2(g_e - g_{ii})B_i$, where $i = a$, b, and c labels the molecule-fixed principal axes, $g_e \approx 2.002319$ is the free-electron g factor, and B_i is the rotational constant.[53] A rigorous calculation of ϵ_{ii} based on analytic second-derivative techniques[44,45] is in good agreement with the experimentally derived values (Table 1) but is nonetheless difficult to interpret physically because it comprises second-order response contributions from an entire manifold of electronic excitations. Nevertheless, we can make a series of approximations to these second-order spin−orbit effects to better understand the most important contributions. Following Stone,[54] we neglect differential orbital overlap to reduce the problem to a sum of single-center, single-electron contributions. Moreover, given that O has a spin−orbit constant much larger than that of C ($\zeta_O/\zeta_C \approx 5$), we consider only contributions from the unpaired spin density localized on the O atom.[16] The largest contributions to ϵ_{ii} will then be from mixing with the lowest excited electronic states of B_2 and A_1 symmetry, i.e., those that result from rotating the one-electron hole in the O($2p_x$) component of the singly occupied $\pi(b_1)$ orbital of the $\tilde{X}^2B_1$ ground electronic state by 90° to overlap the in-plane O($2p_y$) and O($2p_z$) atomic orbitals, respectively. The corresponding single-center, single-perturber approximations for the ϵ_{ii} parameters are

$$\epsilon_{aa} \approx 4\zeta_O A \frac{\rho_X \rho_{B_2}}{\Delta E_{B_2-X}} \quad (4)$$

$$\epsilon_{bb} \approx 4\zeta_O B \frac{\rho_X \rho_{A_1}}{\Delta E_{A_1-X}} \quad (5)$$

$$\epsilon_{cc} \approx 0 \quad (6)$$

where $\zeta_O = -139$ cm^{-1} is the effective spin−orbit constant for O(2p) electrons (assumed equal to the spin−orbit splitting of the $^2\Pi$ state of OH[55]) and A and B are the rotational constants (Table 1). ρ_X, ρ_{B_2}, and ρ_{A_1} are the O atomic spin populations in the ground $\tilde{X}^2B_1$ electronic state, the first excited $^2B_2$ state, and the first excited $^2A_1$ state, respectively. ΔE_{B_2-X} and ΔE_{A_1-X} are the corresponding vertical electronic energies. The unpaired spin densities and vertical energies of these electronic states are listed in Figure 3. The theoretical O spin populations are ρ_X = +0.41, ρ_{B_2} = +0.89, and ρ_{A_1} = +0.29. Substituting these quantities into eqs 4 and 5 yields $\epsilon_{aa} \approx -120$ MHz and $\epsilon_{bb} \approx -4.2$ MHz. The a-axis value is in reasonable agreement (20%) with the measured value, $\epsilon_{aa} = -99.466(3)$ MHz, which indicates that the magnetic anisotropy along this axis is indeed dominated by the quasi-atomic O(2p) electronic orbital angular momentum about the O− C_1 bond, i.e., a simple quenching of the first-order spin−orbit effects observed in the orbitally degenerate ground electronic states of OH ($^2\Pi$) and CH_3O (^2E), which correlate to the ground $^2B_1$ and first-excited $^2B_2$ states in phenoxy.[16] The b-axis estimate reproduces the sign of the measured value, ϵ_{bb} = −13.213(1) MHz, but is a factor of ∼3 too small. A more comprehensive study of the electronic states of phenoxy[26,56] shows that the O($2p_z$) orbital character is in fact dispersed over a number of additional $^2A_1$ excited states with similar vertical energies, so that the single-perturber approximation for this axis is not very accurate. The c-axis magnetic anisotropy is expected

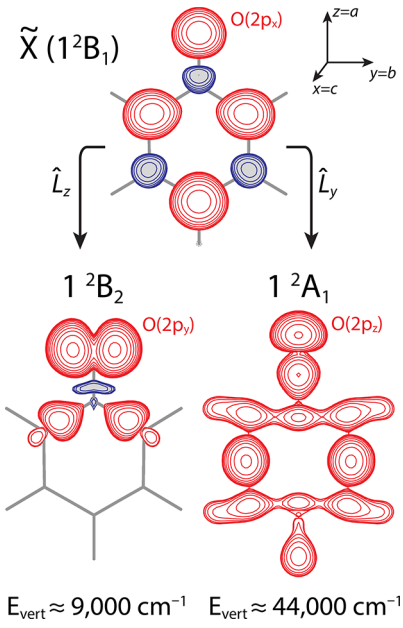

Figure 3. Unpaired spin density of phenoxy. The spin density isosurface (±0.005 au) is shown for the $\tilde{X}^2B_1$ ground electronic state (red contours, positive; blue contours, negative). Spin−orbit interactions about the molecular $z = a$ axis couple the ground state to the low-lying $^2B_2$ state. The corresponding $y = b$ axis interactions couple to much higher lying $^2A_1$ states. The spin density contours and vertical energy of the first excited state of each symmetry are shown at the ROHF-CCSD(T)/cc-pVTZ level of theory.

https://doi.org/10.1021/acs.jpclett.4c00962
J. Phys. Chem. Lett. 2024, 15, 5063−5069

to be small because the O($2p_x$) orbital has zero orbital angular momentum about the $x = c$ axis. Indeed, the small negative measured value, $\epsilon_{cc} = -0.0859(5)$ MHz, reflects the sum of numerous small contributions of both positive and negative signs.

The hyperfine-resolved microwave spectrum of the singly substituted ^{17}O ($I = 5/2$) and ^{13}C ($I = 1/2$) species would provide a complete description of the unpaired spin distribution and heavy-atom structural parameters in phenoxy. The very small natural abundance of ^{17}O (0.04%) will require the use of isotopically enriched discharge precursors, e.g., benzene + $^{17}O_2$ or ^{17}O-labeled anisole. Although the microwave lines of phenoxy are strong enough to observe individual ^{13}C rotational transitions in natural abundance (1%) with long integration times (we estimate 10 h per cavity position), the large number of experimental measurements needed to derive accurate spectroscopic constants makes this approach impractical. A precursor mixture of $^{13}CC_5H_6$ + O_2 would be an efficient strategy for producing all singly substituted ^{13}C species. A similar approach for single-deuterium species (i.e., C_6H_5D + O_2) would provide the necessary data to derive the complete chemical structure. Now that the rotation, spin-rotation, and nuclear hyperfine parameters of the parent isotopologue are accurately known, the isotopically shifted values can be reliably predicted using the theoretical equilibrium geometry and spin-rotation scaling relations.[53] That is, only the hyperfine structure of the substituted nucleus is unconstrained, and its assignment should be straightforward using the theoretical spin densities calculated in this work.

The microwave rest frequencies of phenoxy derived from the best fit parameters in Tables 1 and 2 have an uncertainty of 1−5 kHz for the most intense rotational transitions up to about 40 GHz. This catalog enables studies of phenoxy and its chemistry in both the laboratory and space to be undertaken with considerable confidence. Narrow- and broadband microwave spectroscopy in the centimeter wave region is ideally suited for isomer- and isotopologue-specific detection of phenoxy in complex reactive mixtures at the rotationally cold laboratory conditions achieved in supersonic expansions,[30,57,58] uniform flows,[59−62] and cryogenic buffer-gas-cooled cells.[63]

The cold, dense Taurus molecular cloud (TMC-1) is a well-studied astronomical object that hosts a rich chemical inventory.[64] Two large radio surveys, GOTHAM[32] and QUIJOTE,[31] which target this object in the 8−50 GHz region, have recently revealed several unexpectedly abundant closed-shell mono- and bicyclic aromatic species[65−69] that may represent the first stages of PAH formation. The oxidation chemistry of these and their derived radicals, e.g., phenyl, in molecular clouds, however, is poorly understood. Our results provide the requisite laboratory rest frequencies to undertake a sensitive search for phenoxy in radio surveys of TMC-1. Its detection (or a rigorous upper bound on its column density) could place important constraints on the highly uncertain distribution and abundance of atomic and molecular oxygen in the interstellar medium.[70,71]

Experimental Methods. A dilute mixture of either [0.1% C_6H_6 + 0.2% O_2] or 0.1% anisole in neon at a total pressure of 3.3 bar was expanded from a solenoid valve in 400−500 μs gas pulses at a rate of 5 Hz. As the gas exits the valve, it passes through two copper ring electrodes that differ in potential by 700−1000 V, striking a 20−40 mA discharge when a high gas density is reached. As the gas expands from the discharge volume, it supersonically expands and rapidly cools to a rotational temperature of $T_{rot} \approx 2$ K. At optimal conditions, the anisole precursor produced 2−5× as many phenoxy radicals as the benzene/O_2 mixture.

Rotational transitions of phenoxy were excited by a 1 μs pulse of resonant radiation, and the subsequent FID was detected by a sensitive microwave receiver, sampled by a digital oscilloscope, and Fourier-transformed. Phenoxy has a large permanent dipole moment [$\mu_a \approx 3.7$ D; ROHF-CCSD(T)/cc-pVQZ equilibrium value], and its transitions were detected with a signal-to-noise ratio of 50:1 in 1 min of integration in the most favorable cases (FID exponential filter time constant = 200 μs and instantaneous cavity acquisition bandwidth = 0.3 MHz). Three mutually orthogonal pairs of Helmholtz coils surrounding the vacuum chamber were tuned to null the Earth's magnetic field at the center of the microwave cavity. Zeeman broadening from the residual field at the edges of the cavity volume (<50 mG) prevented the detection of only the weakest and most field-sensitive hyperfine components (i.e., $\Delta F = 0$ transitions, where F is the total angular momentum quantum number). The measured rest frequencies had an accuracy of about 2 kHz.

■ ASSOCIATED CONTENT

Supporting Information

The Supporting Information is available free of charge at https://pubs.acs.org/doi/10.1021/acs.jpclett.4c00962.

Calculated phenoxy equilibrium geometry (Table S1) (PDF)

SPFIT/SPCAT input and output files: phenoxy.lin, experimental line list; phenoxy.par, SPFIT parameter input file; phenoxy.fit, fit results; phenoxy.var, SPCAT parameter input file; phenoxy.int, SPCAT dipole input file; and phenoxy.cat, calculated catalog (ZIP)

■ AUTHOR INFORMATION

Corresponding Authors

P. Bryan Changala − *Center for Astrophysics | Harvard & Smithsonian, Cambridge, Massachusetts 02138, United States;* orcid.org/0000-0003-0304-9814; Email: bryan.changala@cfa.harvard.edu

Michael C. McCarthy − *Center for Astrophysics | Harvard & Smithsonian, Cambridge, Massachusetts 02138, United States;* orcid.org/0000-0001-9142-0008; Email: mccarthy@cfa.harvard.edu

Complete contact information is available at: https://pubs.acs.org/10.1021/acs.jpclett.4c00962

Notes

The authors declare no competing financial interest.

■ ACKNOWLEDGMENTS

This work was supported by the U.S. National Science Foundation Awards AST-1908576, AST-2307137, and PHY-2110489.

■ REFERENCES

(1) Buth, R.; Hoyermann, K.; Seeba, J. Reactions of phenoxy radicals in the gas phase. *Symp. Int. Combust.* **1994**, *25*, 841−849.

(2) Berho, F.; Lesclaux, R. The phenoxy radical: UV spectrum and kinetics of gas-phase reactions with itself and with oxygen. *Chem. Phys. Lett.* **1997**, *279*, 289−296.

(3) Platz, J.; Nielsen, O. J.; Wallington, T. J.; Ball, J. C.; Hurley, M. D.; Straccia, A. M.; Schneider, W. F.; Sehested, J. Atmospheric chemistry of

the phenoxy radical, $C_6H_5O(\cdot)$: UV spectrum and kinetics of its reaction with NO, NO_2, and O_2. *J. Phys. Chem. A* **1998**, *102*, 7964−7974.
(4) Barckholtz, C.; Fadden, M. J.; Hadad, C. M. Computational study of the mechanisms for the reaction of $O_2(^3\Sigma_g)$ with aromatic radicals. *J. Phys. Chem. A* **1999**, *103*, 8108−8117.
(5) Parker, D. S. N.; Kaiser, R. I.; Troy, T. P.; Kostko, O.; Ahmed, M.; Mebel, A. M. Toward the oxidation of the phenyl radical and prevention of PAH formation in combustion systems. *J. Phys. Chem. A* **2015**, *119*, 7145−7154.
(6) Parker, D. S. N.; Zhang, F.; Kaiser, R. I. Phenoxy Radical (C_6H_5O) formation under single collision conditions from reaction of the phenyl radical (C_6H_5, X^2A_1) with molecular oxygen (O_2, $X\ ^3\Sigma g^-$): The final chapter? *J. Phys. Chem. A* **2011**, *115*, 11515−11518.
(7) Frenklach, M. Reaction mechanism of soot formation in flames. *Phys. Chem. Chem. Phys.* **2002**, *4*, 2028−2037.
(8) Scheer, A. M.; Mukarakate, C.; Robichaud, D. J.; Ellison, G. B.; Nimlos, M. R. Radical chemistry in the thermal decomposition of anisole and deuterated anisoles: An investigation of aromatic growth. *J. Phys. Chem. A* **2010**, *114*, 9043−9056.
(9) Friderichsen, A. V.; Shin, E.-J.; Evans, R. J.; Nimlos, M. R.; Dayton, D. C.; Ellison, G. The pyrolysis of anisole ($C_6H_5OCH_3$) using a hyperthermal nozzle. *Fuel* **2001**, *80*, 1747−1755.
(10) Jarvis, M. W.; Daily, J. W.; Carstensen, H.-H.; Dean, A. M.; Sharma, S.; Dayton, D. C.; Robichaud, D. J.; Nimlos, M. R. Direct detection of products from the pyrolysis of 2-phenethyl phenyl ether. *J. Phys. Chem. A* **2011**, *115*, 428−438.
(11) Herbst, E. Chemistry in the interstellar medium. *Annu. Rev. Phys. Chem.* **1995**, *46*, 27−54.
(12) Stone, T. J.; Waters, W. A. Electron spin resonance spectra of transient aryloxy and arylamino free radicals. *Proc. Chem. Soc.* **1962**, *1962*, 253.
(13) Dixon, W. T.; Norman, R. O. C. Electron spin resonance studies of oxidation. Part IV. Some benzenoid compounds. *J. Chem. Soc.* **1964**, *1964*, 4857.
(14) Lloyd, R. V.; Wood, D. E. Free radicals in an adamantane matrix. VIII. EPR and INDO study of the benzyl, anilino, and phenoxy radicals and their fluorinated derivatives. *J. Am. Chem. Soc.* **1974**, *96*, 659−665.
(15) Schuler, R. H.; Neta, P.; Zemel, H.; Fessenden, R. W. Conversion of hydroxyphenyl to phenoxyl radicals: A radiolytic study of the reduction of bromophenols in aqueous solution. *J. Am. Chem. Soc.* **1976**, *98*, 3825−3831.
(16) Bresgunov, A.; Dubinsky, A.; Poluektov, O.; Lebedev, Y.; Prokof'ev, A. The structure of phenoxyl radicals as studied by 2 mm band ESR. *Mol. Phys.* **1992**, *75*, 1123−1131.
(17) Amorati, R.; Pedulli, G. F.; Guerra, M. Hydrogen hyperfine splitting constants for phenoxyl radicals by DFT methods: Regression analysis unravels hydrogen bonding effects. *Org. Biomol. Chem.* **2010**, *8*, 3136.
(18) Gunion, R. F.; Gilles, M. K.; Polak, M. L.; Lineberger, W. Ultraviolet photoelectron spectroscopy of the phenide, benzyl and phenoxide anions, with ab initio calculations. *Int. J. Mass Spec. Ion Proc.* **1992**, *117*, 601−620.
(19) Kim, J. B.; Yacovitch, T. I.; Hock, C.; Neumark, D. M. Slow photoelectron velocity-map imaging spectroscopy of the phenoxide and thiophenoxide anions. *Phys. Chem. Chem. Phys.* **2011**, *13*, 17378.
(20) Richardson, J. H.; Stephenson, L. M.; Brauman, J. I. Photodetachment of electrons from phenoxides and thiophenoxide. *J. Am. Chem. Soc.* **1975**, *97*, 2967−2970.
(21) Dewar, M. J. S.; David, D. E. Ultraviolet photoelectron spectrum of the phenoxy radical. *J. Am. Chem. Soc.* **1980**, *102*, 7387−7389.
(22) Hemberger, P.; da Silva, G.; Trevitt, A. J.; Gerber, T.; Bodi, A. Are the three hydroxyphenyl radical isomers created equal? The role of the phenoxy radical. *Phys. Chem. Chem. Phys.* **2015**, *17*, 30076−30083.
(23) Fernholz, C.; Bodi, A.; Hemberger, P. Threshold photoelectron spectrum of the phenoxy radical. *J. Phys. Chem. A* **2022**, *126*, 9022−9030.
(24) Tonokura, K.; Ogura, T.; Koshi, M. Near-UV absorption spectrum of the phenoxyl radical and kinetics of its reaction with CH_3. *J. Phys. Chem. A* **2004**, *108*, 7801−7805.
(25) Pullin, D.; Andrews, L. The absorption spectra of the phenoxyl radical in solid argon. *J. Mol. Struct.* **1983**, *95*, 181−185.
(26) Radziszewski, J. G.; Gil, M.; Gorski, A.; Spanget-Larsen, J.; Waluk, J.; Mróz, B. J. Electronic states of the phenoxyl radical. *J. Chem. Phys.* **2001**, *115*, 9733−9738.
(27) Araki, M.; Matsushita, Y.; Tsukiyama, K. Laboratory optical spectroscopy of the phenoxy radical as a candidate for diffuse interstellar bands. *Astron. J.* **2015**, *150*, 113.
(28) Spanget-Larsen, J.; Gil, M.; Gorski, A.; Blake, D. M.; Waluk, J.; Radziszewski, J. G. Vibrations of the phenoxyl radical. *J. Am. Chem. Soc.* **2001**, *123*, 11253−11261.
(29) Changala, P. B.; McCarthy, M. C. Hyperfine-resolved rotational spectroscopy of phenyl radical. *J. Phys. Chem. Lett.* **2023**, *14*, 5370−5376.
(30) McCarthy, M. C.; Lee, K. L. K.; Carroll, P. B.; Porterfield, J. P.; Changala, P. B.; Thorpe, J. H.; Stanton, J. F. Exhaustive product analysis of three benzene discharges by microwave spectroscopy. *J. Phys. Chem. A* **2020**, *124*, 5170−5181.
(31) Cernicharo, J.; Agúndez, M.; Kaiser, R. I.; Cabezas, C.; Tercero, B.; Marcelino, N.; Pardo, J. R.; De Vicente, P. Discovery of benzyne, *o*-C_6H_4, in TMC-1 with the QUIJOTE line survey. *Astron. Astrophys.* **2021**, *652*, L9.
(32) McGuire, B. A.; Burkhardt, A. M.; Loomis, R. A.; Shingledecker, C. N.; Lee, K. L. K.; Charnley, S. B.; Cordiner, M. A.; Herbst, E.; Kalenskii, S.; Momjian, E.; Willis, E. R.; Xue, C.; Remijan, A. J.; McCarthy, M. C. Early science from GOTHAM: Project overview, methods, and the detection of interstellar propargyl cyanide ($HCCCH_2CN$) in TMC-1. *Astrophys. J. Lett.* **2020**, *900*, L10.
(33) Grabow, J. U.; Palmer, E. S.; McCarthy, M. C.; Thaddeus, P. Supersonic-jet cryogenic-resonator coaxially oriented beam-resonator arrangement Fourier transform microwave spectrometer. *Rev. Sci. Instrum.* **2005**, *76*, 093106.
(34) Pickett, H. M. The fitting and prediction of vibration-rotation spectra with spin interactions. *J. Mol. Spectrosc.* **1991**, *148*, 371−377.
(35) Neta, P.; Fessenden, R. W. Hydroxyl radical reactions with phenols and anilines as studied by electron spin resonance. *J. Phys. Chem.* **1974**, *78*, 523−529.
(36) Bartlett, R. J.; Watts, J.; Kucharski, S.; Noga, J. Non-iterative fifth-order triple and quadruple excitation energy corrections in correlated methods. *Chem. Phys. Lett.* **1990**, *165*, 513−522.
(37) Raghavachari, K.; Trucks, G. W.; Pople, J. A.; Head-Gordon, M. A fifth-order perturbation comparison of electron correlation theories. *Chem. Phys. Lett.* **1989**, *157*, 479−483.
(38) Watts, J. D.; Gauss, J.; Bartlett, R. J. Open-shell analytical energy gradients for triple excitation many-body, coupled-cluster methods: MBPT(4), CCSD+T(CCSD), CCSD(T), and QCISD(T). *Chem. Phys. Lett.* **1992**, *200*, 1−7.
(39) Gauss, J.; Lauderdale, W. J.; Stanton, J. F.; Watts, J. D.; Bartlett, R. J. Analytic energy gradients for open-shell coupled-cluster singles and doubles (CCSD) calculations using restricted open-shell Hartree−Fock (ROHF) reference functions. *Chem. Phys. Lett.* **1991**, *182*, 207.
(40) Watts, J. D.; Gauss, J.; Bartlett, R. J. Coupled-cluster methods with noniterative triple excitations for restricted open-shell Hartree−Fock and other general single determinant reference functions. Energies and analytical gradients. *J. Chem. Phys.* **1993**, *98*, 8718.
(41) Dunning, T. H. Gaussian basis sets for use in correlated molecular calculations. I. The atoms boron through neon and hydrogen. *J. Chem. Phys.* **1989**, *90*, 1007.
(42) Woon, D. E.; Dunning, T. H. Gaussian basis sets for use in correlated molecular calculations. V. Core-valence basis sets for boron through neon. *J. Chem. Phys.* **1995**, *103*, 4572−4585.
(43) Mills, I. M. Vibration−Rotation Structure in Asymmetric- and Symmetric-Top Molecules. In *Molecular Spectroscopy: Modern Research*; Rao, K. N., Mathews, C. W., Eds.; Academic Press: New York, 1972; Chapter 3.2, pp 115−140, DOI: 10.1016/B978-0-12-580640-4.50013-3.

https://doi.org/10.1021/acs.jpclett.4c00962
J. Phys. Chem. Lett. 2024, 15, 5063−5069

(44) Tarczay, G.; Szalay, P. G.; Gauss, J. First-principles calculation of electron spin-rotation tensors. *J. Phys. Chem. A* **2010**, *114*, 9246−9252.
(45) Szalay, P. G.; Gauss, J. G.; Stanton, J. F. Analytic UHF-CCSD(T) second derivatives: Implementation and application to the calculation of the vibration-rotation interaction constants of NCO and NCS. *Theor. Chem. Acc.* **1998**, *100*, 5−11.
(46) Stanton, J. F.; Gauss, J.; Cheng, L.; Harding, M. E.; Matthews, D. A.; Szalay, P. G. *CFOUR, Coupled-Cluster Techniques for Computational Chemistry*; http://www.cfour.de (accessed April 1, 2023).
(47) Matthews, D. A.; Cheng, L.; Harding, M. E.; Lipparini, F.; Stopkowicz, S.; Jagau, T.-C.; Szalay, P. G.; Gauss, J.; Stanton, J. F. Coupled-cluster techniques for computational chemistry: The CFOUR program package. *J. Chem. Phys.* **2020**, *152*, 214108.
(48) Esselman, B. J.; Zdanovskaia, M. A.; Owen, A. N.; Stanton, J. F.; Woods, R. C.; McMahon, R. J. Precise equilibrium structure of benzene. *J. Am. Chem. Soc.* **2023**, *145*, 21785−21797.
(49) McConnell, H. M. Nuclear and electron magnetic resonance. *Annu. Rev. Phys. Chem.* **1957**, *8*, 105−128.
(50) McConnell, H. M.; Chesnut, D. B. Theory of isotropic hyperfine interactions in π-electron radicals. *J. Chem. Phys.* **1958**, *28*, 107.
(51) McConnell, H. M.; Strathdee, J. Theory of anisotropic hyperfine interactions in π-electron radicals. *Mol. Phys.* **1959**, *2*, 129−138.
(52) Adamo, C.; Subra, R.; Di Matteo, A.; Barone, V. Structure and magnetic properties of benzyl, anilino, and phenoxyl radicals by density functional computations. *J. Chem. Phys.* **1998**, *109*, 10244−10254.
(53) Curl, R. F. The relationship between electron spin rotation coupling constants and *g*-tensor components. *Mol. Phys.* **1965**, *9*, 585−597.
(54) Stone, A. J. Gauge invariance of the *g* tensor. *Proc. R. Soc. A* **1963**, *271*, 424−434.
(55) Beaudet, R. A.; Poynter, R. L. Microwave spectra of molecules of astrophysical interest XII. Hydroxyl radical. *J. Phys. Chem. Ref. Data* **1978**, *7*, 311−362.
(56) Engström, M.; Himo, F.; Gräslund, A.; Minaev, B.; Vahtras, O.; Agren, H. Hydrogen bonding to tyrosyl radical analyzed by ab initio g-tensor calculations. *J. Phys. Chem. A* **2000**, *104*, 5149−5153.
(57) Prozument, K.; Barratt Park, G.; Shaver, R. G.; Vasiliou, A. K.; Oldham, J. M.; David, D. E.; Muenter, J. S.; Stanton, J. F.; Suits, A. G.; Barney Ellison, G.; Field, R. W. Chirped-pulse millimeter-wave spectroscopy for dynamics and kinetics studies of pyrolysis reactions. *Phys. Chem. Chem. Phys.* **2014**, *16*, 15739−15751.
(58) Fritz, S. M.; Mishra, P.; Wullenkord, J.; Fugazzi, P. G.; Kohse-Höinghaus, K.; Zwier, T. S.; Hansen, N. Detecting combustion intermediates via broadband chirped-pulse microwave spectroscopy. *Proc. Combust. Inst.* **2021**, *38*, 1761−1769.
(59) Oldham, J. M.; Abeysekera, C.; Joalland, B.; Zack, L. N.; Prozument, K.; Sims, I. R.; Park, G. B.; Field, R. W.; Suits, A. G. A chirped-pulse Fourier-transform microwave/pulsed uniform flow spectrometer. I. The low-temperature flow system. *J. Chem. Phys.* **2014**, *141*, 154202.
(60) Abeysekera, C.; Zack, L. N.; Park, G. B.; Joalland, B.; Oldham, J. M.; Prozument, K.; Ariyasingha, N. M.; Sims, I. R.; Field, R. W.; Suits, A. G. A chirped-pulse Fourier-transform microwave/pulsed uniform flow spectrometer. II. Performance and applications for reaction dynamics. *J. Chem. Phys.* **2014**, *141*, 214203.
(61) Gurusinghe, R. M.; Dias, N.; Krueger, R.; Suits, A. G. Uniform supersonic flow sampling for detection by chirped-pulse rotational spectroscopy. *J. Chem. Phys.* **2022**, *156*, 014202.
(62) Hearne, T. S.; Abdelkader Khedaoui, O.; Hays, B. M.; Guillaume, T.; Sims, I. R. A novel Ka-band chirped-pulse spectrometer used in the determination of pressure broadening coefficients of astrochemical molecules. *J. Chem. Phys.* **2020**, *153*, 084201.
(63) Porterfield, J. P.; Satterthwaite, L.; Eibenberger, S.; Patterson, D.; McCarthy, M. C. High sensitivity microwave spectroscopy in a cryogenic buffer gas cell. *Rev. Sci. Instrum.* **2019**, *90*, 053104.
(64) Gratier, P.; Majumdar, L.; Ohishi, M.; Roueff, E.; Loison, J. C.; Hickson, K. M.; Wakelam, V. A new reference chemical composition for TMC-1. *Astrophys. J. Suppl. Ser.* **2016**, *225*, 25.
(65) McGuire, B. A.; Burkhardt, A. M.; Kalenskii, S.; Shingledecker, C. N.; Remijan, A. J.; Herbst, E.; McCarthy, M. C. Detection of the aromatic molecule benzonitrile (c-C_6H_5CN) in the interstellar medium. *Science* **2018**, *359*, 202−205.
(66) McGuire, B. A.; Loomis, R. A.; Burkhardt, A. M.; Lee, K. L. K.; Shingledecker, C. N.; Charnley, S. B.; Cooke, I. R.; Cordiner, M. A.; Herbst, E.; Kalenskii, S.; Siebert, M. A.; Willis, E. R.; Xue, C.; Remijan, A. J.; McCarthy, M. C. Detection of two interstellar polycyclic aromatic hydrocarbons via spectral matched filtering. *Science* **2021**, *371*, 1265−1269.
(67) Burkhardt, A. M.; Lee, K. L. K.; Changala, P. B.; Shingledecker, C. N.; Cooke, I. R.; Loomis, R. A.; Wei, H.; Charnley, S. B.; Herbst, E.; McCarthy, M. C.; McGuire, B. A. Discovery of the pure polycyclic aromatic hydrocarbon indene (*c*-C_9H_8) with GOTHAM observations of TMC-1. *Astrophys. J. Lett.* **2021**, *913*, L18.
(68) Cernicharo, J.; Agúndez, M.; Cabezas, C.; Tercero, B.; Marcelino, N.; Pardo, J. R.; De Vicente, P. Pure hydrocarbon cycles in TMC-1: Discovery of ethynyl cyclopropenylidene, cyclopentadiene, and indene. *Astron. Astrophys.* **2021**, *649*, L15.
(69) Sita, M. L.; Changala, P. B.; Xue, C.; Burkhardt, A. M.; Shingledecker, C. N.; Lee, K. L. K.; Loomis, R. A.; Momjian, E.; Siebert, M. A.; Gupta, D.; Herbst, E.; Remijan, A. J.; McCarthy, M. C.; Cooke, I. R.; McGuire, B. A. Discovery of interstellar 2-cyanoindene (2-C_9H_7CN) in GOTHAM observations of TMC-1. *Astrophys. J. Lett.* **2022**, *938*, L12.
(70) Black, J. H.; Smith, P. L. Interstellar O_2. I—Abundance, excitation, and prospects for detection of $^{16}O^{18}O$ at radio frequencies. *Astrophys. J.* **1984**, *277*, 562.
(71) Whittet, D. C. B. Oxygen depletion in the interstellar medium: Implications for grain models and the distribution of elemental oxygen. *Astrophys. J.* **2010**, *710*, 1009−1016.

https://doi.org/10.1021/acs.jpclett.4c00962
J. Phys. Chem. Lett. 2024, 15, 5063−5069